catalysts

MDPI

Article

Microwave-Assisted Biodiesel Production Using Activated Oat Hull-Derived Biochar as Catalyst

Jaime Ñanculeo [1], Benjamín Nahuelcura [1], Mara Cea [2,3], Norberto Abreu [2,3], Karla Garrido-Miranda [3], Sebastián Meier [4,5], Juan Miguel Romero-García [6] and María Eugenia González [2,3,*]

1 Doctoral Program in Engineering Sciences with Specialization in Bioprocesses, University of La Frontera, Av. Francisco Salazar 01145, Temuco 4780000, Chile; jaime.nanculeo@ufrontera.cl (J.Ñ.); benjamin.nahuelcura@ufrontera.cl (B.N.)
2 Department of Chemical Engineering, University of La Frontera, Temuco 4780000, Chile; mara.cea@ufrontera.cl (M.C.); norberto.abreu@ufrontera.cl (N.A.)
3 Scientific and Technological Bioresources Nucleus-BIOREN, University of La Frontera, Temuco 4780000, Chile; karla.garrido@ufrontera.cl
4 Instituto de Investigaciones Agropecuarias INIA Carillanca, Casilla Postal 58-D, Temuco 4880815, Chile; sebastian.meier@inia.cl
5 Escuela de Agronomía, Facultad de Ciencias, Ingeniería y Tecnología, Universidad Mayor, Campus Alemania Sede Temuco, Temuco 4801043, Chile
6 Department of Chemical, Environmental and Materials Engineering, Institute of Biorefineries Research (I3B), Universidad de Jaén, 23001 Jaen, Spain; jrgarcia@ujaen.es
* Correspondence: mariaeugenia.gonzalez@ufrontera.cl

Abstract

This study investigated the effect of KOH activation on biochar, with a focus on how porosity and potassium content influence microwave-assisted catalytic biodiesel production, using experimental design approaches. Activated biochar was synthesized from oat hull waste through KOH activation, followed by pyrolysis under controlled conditions. The biochar was characterized through chemical, morphological, and physical analyses, and its catalytic performance in converting used waste cooking oil (WCO) into biodiesel was evaluated using methanol as the acyl acceptor and microwave irradiation to optimize the reaction via experimental design. Results revealed that increasing the KOH/biomass ratio significantly enhanced the specific surface area (SSA) of the catalyst, achieving a maximum SSA of 637.28 m^2/g under optimal pyrolysis conditions: 600 °C for 3 h with a KOH/biomass ratio of 2. A maximum fatty acid methyl ester (FAME) yield of 100% was achieved within 1 min of microwave-assisted reaction using an optimized catalyst dosage of 2.5%, a WCO/MeOH molar ratio of 1/12, and a reaction temperature of 150 °C, with the catalyst being successfully recycled across three cycles. An economic and energy evaluation estimated a catalyst production cost of USD 176.97/kg and a biodiesel production cost of USD 8.9/kg of FAMEs. This research provides a straightforward and cost-effective approach for biofuel production.

Keywords: biochar-based alkaline catalyst; activated biochar; microwave irradiation; waste cooking oil; transesterification; biodiesel

Academic Editors: Na Chen and Kecheng Zhu

Received: 20 February 2025
Revised: 30 March 2025
Accepted: 30 March 2025
Published: 31 July 2025

Citation: Ñanculeo, J.; Nahuelcura, B.; Cea, M.; Abreu, N.; Garrido-Miranda, K.; Meier, S.; Romero-García, J.M.; González, M.E. Microwave-Assisted Biodiesel Production Using Activated Oat Hull-Derived Biochar as Catalyst. *Catalysts* **2025**, *15*, 729. https://doi.org/10.3390/catal15080729

1. Introduction

Diversifying the energy matrix to adopt cleaner sources is a global imperative. Currently, approximately 80% of the world's energy demand is supplied by fossil fuels [1], which results in significant greenhouse gas (GHG) emissions that severely impact the environment [2]. These emissions also pose health risks, as air pollution is estimated to cause

10.2 million deaths annually, mostly children and the elderly with respiratory diseases [3]. Although the Paris Agreement aims to limit global warming to 1.5 °C above pre-industrial levels to avert catastrophic consequences [4], projections indicate this threshold may be exceeded by 2030 due to persistent reliance on fossil fuels [5]. This scenario underscores the urgent need for sustainable energy alternatives. One alternative is biodiesel, a biofuel composed of fatty acid methyl esters produced via the transesterification of plants or animal-derived lipids [6]. Biodiesel offers several advantages, including production from renewable resources and waste valorization, lower GHG emissions, biodegradability, compatibility with diesel engines, and enhanced lubricating properties [7,8]. While it is primarily derived from natural feedstocks such as palm oil [9] and soybean [10], biodiesel can also be produced from waste materials, such as waste cooking oil (WCO), making it an environmentally friendly biofuel [11]. Catalysts for biodiesel production are generally classified as homogeneous or heterogeneous based on their phase. Homogeneous catalysts, such as KOH and NaOH, are cost-effective and efficient; however, they exhibit significant drawbacks, including product separation challenges, high saponification rates, and the need for extensive neutralization and washing processes, which generate large volumes of effluents [12]. In contrast, heterogeneous catalysts provide a more sustainable and efficient alternative, easily separable, reusable, and produce fewer by-products and liquid wastes [13]. They also exhibit higher tolerance to impurities in feedstocks, enabling the use of low-cost crude or waste oils and reducing reactor corrosion [14]. To achieve faster production and catalyst reusability, developing low-cost, eco-friendly heterogeneous catalysts is crucial. Thermochemical waste valorization offers a sustainable pathway to produce materials, employing techniques like combustion, gasification, and pyrolysis [15]. Combustion is an exothermic process in which biomass is thermally degraded in excess oxygen, generating heat and stable gases such as CO_2 [16]. Gasification, on the other hand, occurs in oxygen-limited environments at temperatures between 700 and 1200 °C, producing syngas rich in H_2 and CH_4 [17]. Both processes yield ash as a solid by-product, which is characterized by high inorganic content and low surface area [18]. In contrast, pyrolysis is an endothermic process conducted in an inert atmosphere (typically with oxygen replaced by N_2), wherein lignocellulosic residues are thermally degraded to produce syngas, bio-oil, and biochar [19]. The main characteristics of biochar are its low ash content, high surface area, functional groups, and its origin from renewable resources through waste valorization [20]. These properties have expanded their applications in fields such as soil amendment [21], heterogeneous catalysis [22], adsorption [23], and gas purification [24]. In biodiesel production, biochar has demonstrated promising catalytic properties. For example, Jung et al. [25] reported a 95% fatty acid methyl ester (FAME) yield using biochar derived from WCO at 350 °C [25]. Similarly, a biochar-based catalyst with Mo/Ni oxides achieved a 74% yield within 2 h, attributed to the active sites in the material [26]. The porous structure of biochar enhances the interaction between lipids and methanol by facilitating reactant collisions within the pores, especially at elevated temperatures. However, both homogeneous and heterogeneous catalysts have key limitations in biodiesel production, mainly in the need to reduce reaction times, improve yields, and increase the contact area with the reactants. Homogeneous catalysts, although highly reactive, require long purification processes and generate large volumes of effluent, which affect process efficiency. On the other hand, heterogeneous catalysts, although reusable and more sustainable, tend to have lower catalytic activity, which implies higher temperatures and longer reaction times to achieve efficient conversions. In addition, their low dispersion in the medium reduces interaction with the reagents [27]. Therefore, the novelty of this research lies in the production of biodiesel using biochar of high surface area and reusability as a catalyst for the microwave-assisted transesterification reaction. The effectiveness of the

transesterification reaction can be enhanced using microwave-assisted technology, which improves heat transfer to the reaction medium, enhancing the interaction of the reactants and considerably decreasing the reaction time [28]. This technique has demonstrated greater efficiency compared to traditional heating by reducing by-product generation and enhancing biodiesel production [29]. Nevertheless, the integration of biochar as a heterogeneous catalyst with microwave-assisted transesterification has still not been thoroughly investigated, emphasizing the necessity for more optimization. This improves biodiesel production by increasing reaction yield, energy consumption, reaction time, and waste recycling, which are key factors for future scalability of the process [30]. In this context, this research focused on the development of a porous biochar catalyst derived from oat hulls and its application in the production of biodiesel by microwave-assisted transesterification, as an alternative for the valorization of WCO.

2. Results and Discussion

Table 1 summarizes the main experimental results for biochar activation: specific surface area total (Y_{BET}, in m^2/g), total pore volume (Y_{Vp} in cm^3/g), and average pore size (Y_{Pd} in nm). Using experimental data, the relationships between the factors (X_1, X_2, and X_3) and the response Y_{BET} were analyzed through an ANOVA test, as shown in Table 2. The best-fitting response function for the significant main effects and interactions for the Y_{BET} is represented by Equation (1):

$$Y_{BET} = 238.56 + 78.89A + 90.99B + 65.62C - 8.84AB + 197.26AC - 2.66BC + 88.9ABC \quad (1)$$

where A, B, and C are coded factors of temperature, residence time, and KOH/biomass ratio, respectively, according to Equations (2)–(4):

$$A = \frac{X_1 - 401}{100} \quad (2)$$

$$B = X_2 - 2 \quad (3)$$

$$C = \frac{X_3 - 1.5}{1.25} \quad (4)$$

Table 1. Experimental results obtained from the factorial design for activated biochar (AB) production.

Run	Identification Sample	Y_{BET} (m^2/g)	Y_{Vp} (cm^3/g)	Y_{Pd} (nm)
1	AB1	411.94	0.40	3.51
2	AB2	99.91	0.17	4.17
3	AB3	87.56	0.11	3.84
4	AB4	36.30	0.06	3.93
5	AB5	482.71	0.70	3.33
6	AB6	131.45	0.28	3.97
7	AB7	50.49	0.07	4.07
8	AB8	119.02	0.18	3.97
9	AB9	19.75	0.05	4.94
10	AB10	637.28	0.348	3.10
11	AB11	58.65	0.01	4.09

Table 2. Significance test results of factors and interactions for the models of activated biochar (AB).

Factors or Interactions	*p*-Value of Factors of Y_{BET}
A	0.0101 *
B	0.0076 *
C	0.0145 *
AB	0.3842
AC	0.0016 *
BC	0.7709
ABC	0.0080 *
Model	0.0068 *
R^2	0.9981

* Significant.

2.1. Effect of Pyrolysis Process Conditions on the Porosity of Biochar

Figure 1 illustrates the three-dimensional response surface plots for the SSA of the activated biochar, highlighting the interactions between key variables. The plots depict the effects of temperature (X_1) and residence time (Rt) (X_2) (Figure 1a), temperature (X_1) and KOH/biomass ratio (X_3) (Figure 1b), and residence time (X_2) and KOH/biomass ratio (X_3) (Figure 1c). The interaction between temperature and residence time shows a directly proportional relationship with the SSA of the activated biochar (Figure 1a). However, the most significant enhancement in SSA is observed with the interaction between temperature and KOH/biomass ratio (Figure 1b), as the maximum SSA value is achieved at higher temperatures and KOH/biomass ratios.

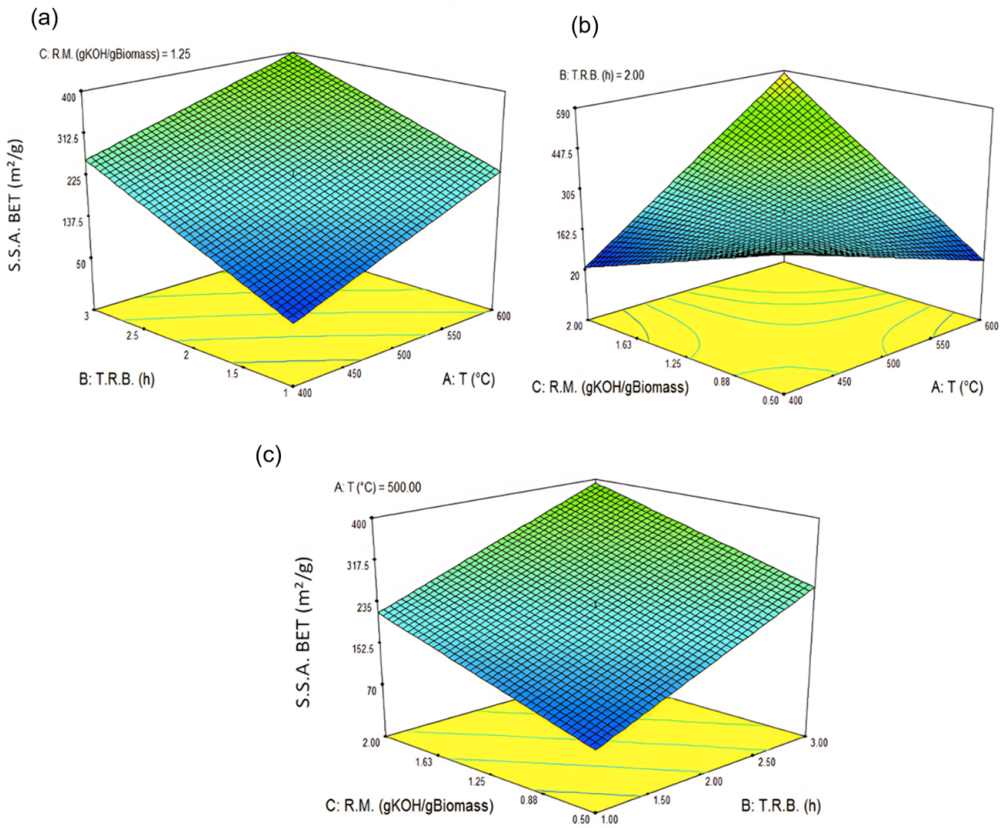

Figure 1. Effects on SSA ($p < 0.05$) produced by (**a**) temperature vs. residence time (at 1.25 KOH/biomass ratio), (**b**) temperature vs. KOH/biomass ratio (at 2 h Rt), and (**c**) KOH/biomass ratio vs. residence time (at 500 °C).

This phenomenon occurs due to the intensified pore widening and the removal of external carbon atoms during carbon gasification at elevated temperatures [31]. Based on other experimental studies, the reactions involved in the activation process by KOH are as follows (Equations (6)–(10)) [32]:

$$6KOH + 2C \rightarrow 2K_2CO_3 + 2K + 3H_2 \quad (5)$$

The reactions outlined illustrate how biomass and its functional groups interact with KOH, leading to the formation of K_2CO_3 (Equation (5)), which acts as the primary precursor for pore development in biochar. At elevated temperatures (600–800 °C), K_2CO_3 decomposes into K_2O and K, releasing CO or CO_2. In this study, the highest SSA was achieved primarily due to K_2CO_3 formation; however, further optimization could be achieved by increasing the KOH content or pyrolysis temperature. Additionally, KOH activation promotes the development of hierarchically porous structures, characterized by a high density of micropores resulting from the efficiency of KOH impregnation and carbon volatilization as CO and CO_2 [32]. Samples produced at less intense pyrolysis conditions (400 °C) have a low Y_{Vp} (less than 0.1 cm^3/g) and a higher Y_{Pd} (greater than 4 nm), which are due to the low carbonization and volatile compound content [32]. However, as the intensity of the factors studied increases, an increment in the Y_{Vp} is observed due to the increase in pore depth, and a decrease in the Y_{Pd} is due to the formation of micropores in the carbonaceous structure [31]. This pore development allows the mass transfer involved in biodiesel production to be improved by increasing available active sites. Adsorption–desorption isotherms and pore size distribution curves are presented in the Supplementary Materials (Figure S1 and Figure S2, respectively).

2.2. Effect of Chemical Activation on Catalyst Morphology

SEM images (Figure 2) reveal the structural transformation of the biomass following the activation process. The alkaline treatment of oat hulls, combined with biochar production, resulted in the development of microporosity, with most samples exhibiting an amorphous structure distinct from biochar derived from untreated oat hulls. The composition of oat hulls can significantly influence the resulting biochar structure. For instance, raw materials with high lignin content typically yield macroporous biochar, whereas those with high cellulose content promote the formation of both macro- and microporous structures [31,32]. Non-activated biochar B600 (Figure 2a) displays a rough surface with limited porosity, which restricts reactant dissolution and confines catalysis to surface reactions. Conversely, the activated biochar samples AB10 (Figure 2b) and AB5 (Figure 2c) exhibit a well-developed interconnected pore system comprising individual cylindrical pores, typical of KOH-activated biochars [33–36]. SEM analysis also indicates that activation contributes to pore widening and the opening of macropore channels. This pore structure underscores the role of micropores in determining the surface area and volume of carbon catalysts, while meso- and macropores facilitate reactant diffusion [37]. The pore openings and channel sizes are particularly significant due to the dimensions of the molecules involved in the reaction, such as triglycerides, which measure approximately 0.8 nm [38]. Hierarchically porous and interconnected biochar improves the diffusion of the triglyceride (TG)–MeOH system within the carbonaceous matrix (Figure 2d), enhancing accessibility to the surface area created by KOH activation. This increased accessibility is crucial for boosting the reaction rate [39].

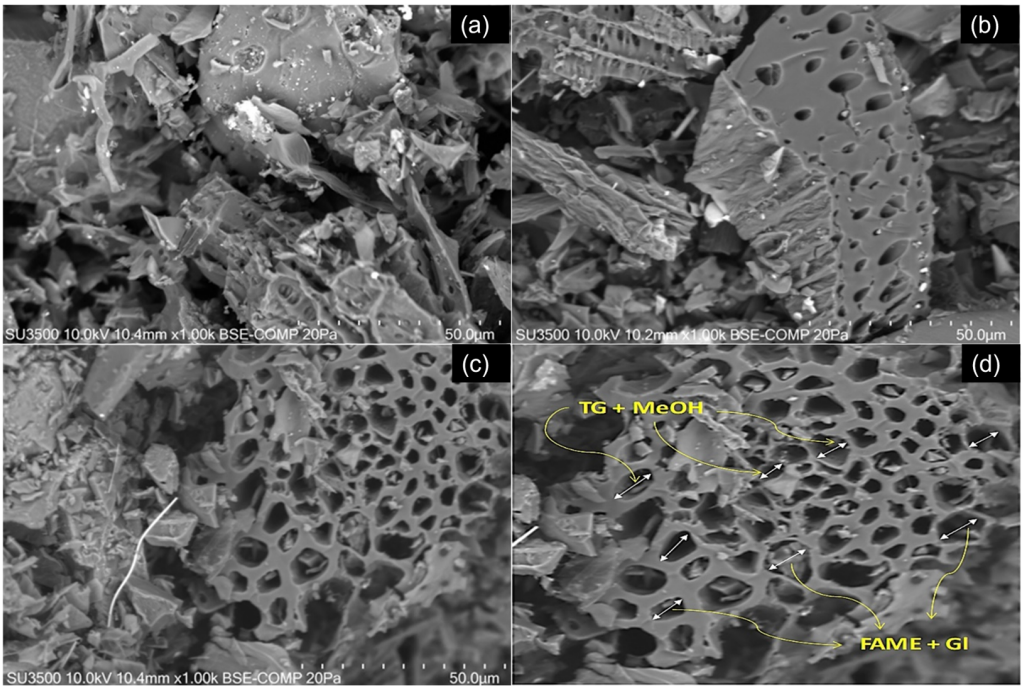

Figure 2. SEM images of (**a**) non-activated biochar pyrolyzed at T = 600 °C, Rt = 3 h (B600); (**b**) activated biochar from treated biomass and subsequent pyrolysis at T = 600 °C, Rt = 3 h, and KOH/biomass ratio = 2 (AB10); (**c**) activated biochar from treated biomass and subsequent pyrolysis at T = 400 °C, Rt = 3 h, and KOH/biomass ratio 0.5 (AB5); and (**d**) schematic representation of reactants and products diffusion through the macropores within the activated catalysts.

According to the model, the optimal conditions for maximizing the SSA of activated biochar (AB) are a temperature of 600 °C, a residence time of 3.0 h, and a KOH/biomass ratio of 2.0. To validate the model, experiments were conducted under these conditions, and the SSA was measured. The experimental results and model predictions are summarized in Table 3, showing a difference of less than 14.9% in BET SSA between the experimental and predicted values. This discrepancy can be attributed to the inherent heterogeneity of the pre-activated biomass.

Table 3. Predicted and experimental values for SSA of activated biochar synthesized at T = 600 °C, Rt = 3.0 h, and KOH/biomass ratio = 2.0.

Parameters	Predicted by Model	Experimental Value
Specific surface area (SSA) BET for AB (m^2/g)	748.63	637.28 ± 8.32

2.3. Effect of Activation Process Conditions in the Composition of Activated Biochar

The chemical composition of the biochar produced in the experimental design is summarized in Table 4. Literature indicates that temperature has the most significant effect on biochar composition. However, in this study, it is challenging to isolate the effect of a single parameter due to the interactions among the three parameters investigated. When the pretreated biomass was exposed to higher temperatures (600 °C) and extended residence times (3 h), a reduction in carbon content (C) was observed compared to untreated biochar (B600). For example, AB7 (activated biochar at 600 °C for 3 h with a KOH/biomass ratio of 2) exhibited a carbon content of 59%, whereas AB3 (activated biochar at 400 °C for 0.5 h with a KOH/biomass ratio of 0.5) had a carbon content of 76.7%. Additionally, oxygen content increased, while hydrogen content did not display a consistent trend

with temperature. As described in the reviewed activation reactions, KOH activation of lignocellulosic biomass promotes the formation of K_2CO_3 at approximately 750 K (476 °C) within the matrix [38]. Furthermore, the reaction between KOH and carbon facilitates the intercalation of potassium metal into the biochar layers, resulting in an expanded porous structure. This process, driven by the deposition of potassium salts on the biochar surface, reduces the overall carbon content [39].

Table 4. Results of elemental analysis for activated biochar (AB) and the control (biochar pyrolyzed at 600 °C without activation).

Samples		Elemental Analysis					Ash (%)
		%C	%H	%N	%S	%O	
Activated biochar (AB)	AB1	71.2	2.0	0.8	n.d.	15.2	10.8
	AB2	73.2	2.1	1.0	n.d.	16.0	7.7
	AB3	75.6	2.3	1.2	n.d.	14.2	6.7
	AB4	74.3	2.4	1.2	n.d.	15.9	6.2
	AB5	76.2	1.9	1.0	n.d.	14.0	6.9
	AB6	74.8	2.0	1.4	n.d.	15.8	6.0
	AB7	71.7	2.0	0.9	n.d.	17.9	9.9
	AB8	71.0	2.7	1.3	n.d.	18.6	6.4
	AB9	74.3	2.6	1.4	n.d.	18.6	3.1
	AB10	78.1	2.2	1.2	n.d.	13.4	5.1
	AB11	74.8	2.3	1.4	n.d.	15.6	5.9
Biochar pyrolyzed at 600 °C	B600	78.3	4.7	1.9	n.d.	5.3	9.8

n.d.: not detected.

2.4. Biodiesel Production

To study the catalytic activity of activated biochar, the conversion of waste cooking oil into biodiesel using methanol as acyl acceptor was evaluated using microwave-assisted irradiation.

The catalyst used for biodiesel production was activated biochar obtained from the experiments used to validate the model (Table 1). The surface characteristics and potassium content are shown in Table 5. The potassium content of the non-activated biochar sample (B600) corresponds to the original K content present in the raw material (oat hulls) [40,41], which is due to cultivation conditions, such as soil type and fertilization, among others [42].

Table 5. Surface characteristics of the material used as catalyst.

Material	SSA BET (m^2/g)	Pore Volume (cm^3/g)	Average Pore Diameter (nm)	Potassium Content (%)
B600	108.28	0.008	2.24	1.72
AB	637.28	0.348	1.10	9.40

The evaluation of the transesterification process over time using AB as a catalyst is shown in Figure 3. The results indicate that the maximum FAME yield was achieved within one minute of reaction, reaching a conversion rate of approximately 63%. No significant increase in yield was observed with longer reaction times. In contrast, when non-activated biochar (B600) was used as a catalyst, the conversion to FAME was nearly negligible.

This outcome highlights the catalytic effect of potassium present on the surface of the activated biochar.

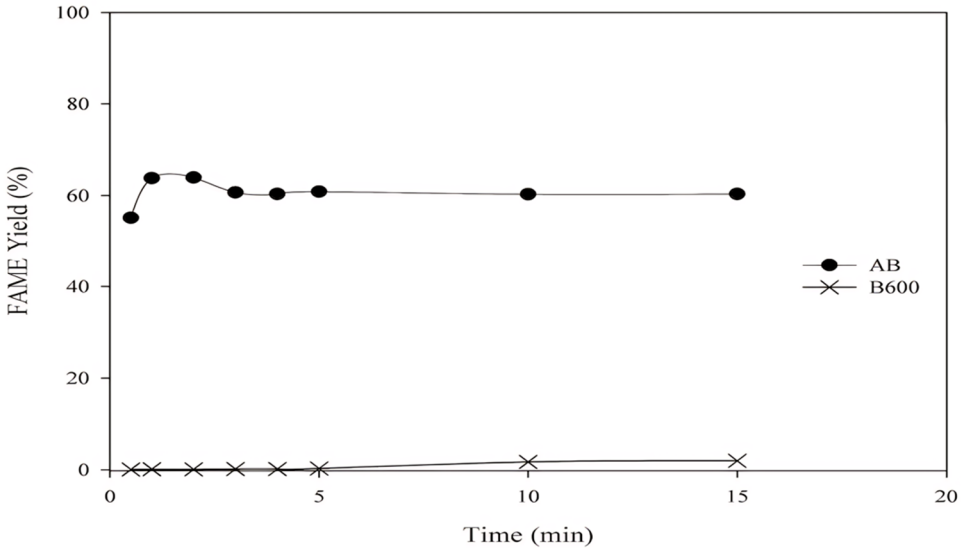

Figure 3. FAME conversion in the time using activated biochar (AB) and non-activated biochar (B600) as catalysts in the microwave reactor. The conditions for performing the transesterification trials were a waste cooking oil/methanol molar ratio of 1/10, 10% catalyst dosage relative to the oil mass, and a temperature of 200 °C.

Triglyceride transesterification to FAMEs in the presence of acid catalysts has been reported by several researchers [43,44]. It has been widely accepted that this reaction occurs according to the stoichiometric reaction displayed in Figure 4.

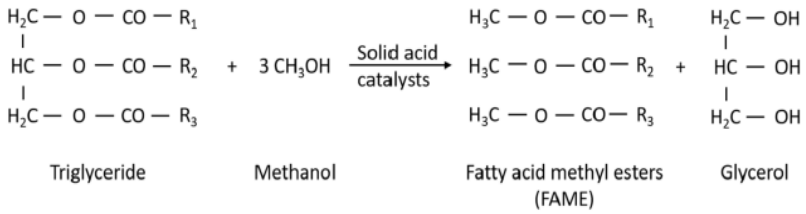

Figure 4. Catalytic transesterification of triglyceride to FAMEs.

In our previous studies [43], it was reported that this reaction appears to follow a pseudo-first-order kinetic model based on TG concentration until maximum conversion is achieved in the presence of the synthesized catalyst. In this case, when using the AB catalyst, the maximum FAME concentration was reached within one minute, after which the FAME concentration remained almost stable. Similar results, but with longer reaction times, were obtained by [45]. In this context, the kinetics of triglyceride transesterification to FAMEs using the AB catalyst can be attributed to an Eley–Rideal heterogeneous model, as outlined by the following reaction mechanism ("*" represents an active site) [45] in Equations (7)–(9):

$$TG + * \rightarrow TG* \text{ (triglyceride adsorption on the catalyst)} \quad (6)$$

$$TG* + 3MeOH + 3* \leftrightarrow 3FAME* + Gl* \text{ (surface transesterification of TG)} \quad (7)$$

$$3FAME* \leftrightarrow FAME + 3* \text{ (FAME desorption from the catalyst)} \quad (8)$$

$$Gl* \leftrightarrow Gl + * \text{ (glycerol desorption from the catalyst surface)} \quad (9)$$

In this mechanism, the primary active sites described could be associated with the basic sites generated by the KOH activation process [46,47]. In this context, the differences in FAME conversion can be explained by the fact that, in the case of non-activated biochar, the reaction appeared to occur homogeneously, involving only the reactants in the bulk solution. However, the KOH-activated biochar exhibited more efficient catalytic activity due to its increased surface area and the greater availability of basic active sites, such as the formation of K_2O and K_2CO_3, which facilitate the deprotonation of methanol and the subsequent formation of the methoxide anion (CH_3O^-), a key intermediate in transesterification [48]. Although biochar activation with KOH is more effective at temperatures above 700 °C in terms of surface area enhancement, the availability of basic sites decreases significantly due to the release of CO/CO_2 [32]. Additionally, the reaction is further enhanced through microwave-assisted transesterification, which occurs due to the selective absorption of microwave radiation by methanol (loss tangent = 0.659). As a dipolar molecule, methanol undergoes uniform heating with increased molecular vibration, leading to a reduction in the activation energy of the reaction [49]. This effect facilitates the cleavage of ester bonds in triglycerides, promoting their conversion into mono- and diacylglycerides until the formation of FAMEs [50].

According to the FAME conversion obtained, similar studies have been reported by Patil et al. [51], where microwave technology was used to produce biodiesel from waste frying oil using 2% KOH as catalyst, methanol as acyl acceptor, and a temperature of 60 °C, achieving conversions of up to 92% after 6 min [51]. Additionally, Hincapié et al., reported a conversion of 80.1% of castor oil into biodiesel using microwave technology with a lower catalyst concentration (1.5% KOH), ethanol as acyl acceptor, and 60 °C over a longer period (10 min) [52]. The reduced time observed in the present study could be attributed to the higher temperature used (150 °C) and the ability of biochar to absorb microwave energy and convert it into heat due to its dielectric properties [53]. Yadav et al. studied microwave-assisted biodiesel production using, as a catalyst, biochar derived from bamboo and derived from coconut husk activated with H_3PO_4 at 400 °C, with a surface area of 10.83 m^2/g, obtaining a yield of 99.6% in the production of biodiesel, at 80 °C for 40 min, using a molar ratio of 1:9 oleic acid to methanol [28]. Another way to use biochar as a catalyst is by functionalization with sulfonic acid, as Devasan et al., who valorized banana peel and obtained a yield of 97.9% at 80 °C for 55 min [54].

2.5. Optimization of Microwave-Assisted Biodiesel Production Using Activated Biochar as a Catalyst

Once the reaction time was established, the effects of temperature (T), catalyst dosage (C), and WCO/MeOH molar ratio (R) on the FAME yield were evaluated using a factorial design. The results of the biodiesel yield under various operating conditions, along with the statistical analyses (ANOVA), are summarized in Table 6. The significance of each parameter was assessed through its probability value (*p*-value). At a 95% confidence level, *p*-values below 0.05 indicated statistically significant effects of the evaluated parameters.

For the response (Y_{FAME}, %), the program delivered a regression model, which included the linear and interaction terms. The model for Y_{FAME}, after performing the experiments and discarding the insignificant effects, can be described as shown in Equation (10):

$$Y_{FAME\ \%} = 79.67 - 1.89A - 19.10B + 32.54C - 33.45AB \quad (10)$$

where A, B, and C are the coded factors of temperature (T), catalyst dosage (C), and WCO/MeOH molar ratio (R), respectively. The coded factors were determined according to Equations (11)–(13):

$$A = (X_1 - 200)/50 \quad (11)$$

$$B = (X_2 - 6.25)/3.75 \quad (12)$$

$$C = (X_3 - 30)/18 \quad (13)$$

The high R^2 value (0.9895) shows the reliability of the regression model for predicting the FAME yield. This was also reflected in the predicted value and the experimental validation value of FAME yield in the model, which was 100%. The optimized mathematical model used to obtain higher FAME yield values requires the use of the following parameter values: T = 150 °C, C = 2.5%, and R = 1:12.

Table 6. Experimental results and statistical analyses obtained from the factorial design for biodiesel production using activated biochar.

Run	Identification Sample	Y_{FAME} (%)
1	B1	84
2	B2	59
3	B3	100
4	B4	100
5	B5	55
6	B6	94
7	B7	65
8	B8	61
9	B9	84
10	B10	64
11	B11	100
12	B12	100
13	B13	100
14	B14	83
15	B15	59
Factor or interactions	p-value of Y_{FAME}	
A	0.0185 *	
B	<0.0001 *	
C	<0.0001 *	
AB	<0.0001 *	
Model	<0.0001 *	
R^2	0.9895	

* Significant.

2.6. Effect of Operational Conditions on Biodiesel Yield

As illustrated in Figure 5a, the FAME yield increased with higher temperatures; however, no significant changes were observed regarding the amount of catalyst at a WCO/MeOH molar ratio of 1:30. This behavior can be attributed to the higher reaction temperature, which enhances the kinetic energy of the reactants, thereby accelerating the mass transfer rate between the oil–methanol and catalyst phases and resulting in maximum conversion [55]. At a constant temperature of 200 °C, the interaction between the WCO/MeOH molar ratio and catalyst dosage increased the FAME yield (Figure 5b). Among these, the WCO/MeOH molar ratio was the most influential factor in the reaction. Similar results have been reported by Kataria et al. [55], who demonstrated that increasing the WCO/MeOH ratio from 1/3 to 1/12 resulted in higher biodiesel yields, achieving a maximum yield of 100% at a 1/12 ratio. In this study, higher WCO/MeOH molar ratios (1/12 to 1/48) were tested to achieve a higher conversion degree. However, it was found that ratios of 1/30 and 1/48 negatively affected the FAME yield, possibly due to biodiesel emulsification, as the solubility of glycerol in methanol increases at higher ratios [55]. When

the catalyst dosage was fixed (Figure 5c), the WCO/MeOH molar ratio remained the most significant factor influencing biodiesel production.

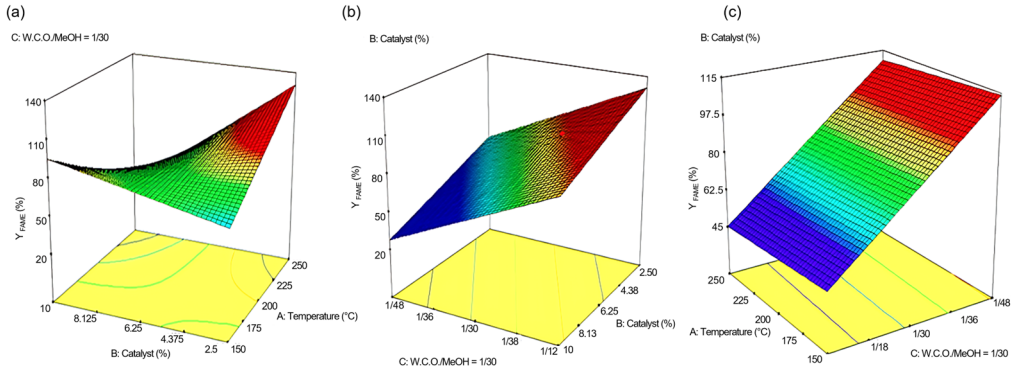

Figure 5. Effect on FAME yield produced by (**a**) temperature and catalyst dosage ($p < 0.05$) (at WCO/MeOH molar ratio: 1/30); (**b**) catalyst dosage and WCO/MeOH molar ratio ($p < 0.05$) (at T = 200 °C); and (**c**) WCO/MeOH molar ratio and temperature ($p < 0.05$) (at catalyst dosage of 6.25%).

2.7. Catalyst Reuse

The reutilization of the catalyst under practical applications is a critical factor, especially given the heterogeneous kinetic mechanism proposed for the reaction. To evaluate this, multiple consecutive runs were conducted under the same conditions used for model validation: 1 min at 150 °C, with 2.5% catalyst and a 1:12 WCO/MeOH molar ratio. The solid catalyst was recovered after each reaction cycle, with three successive runs carried out to assess reusability, both with and without a washing step.

When washing was applied, the catalyst was separated from the reaction mixture by centrifugation, washed twice with methanol under agitation, dried at 100 °C for 2 h, and reused in the subsequent cycle. The performance results are depicted in Figure 6a.

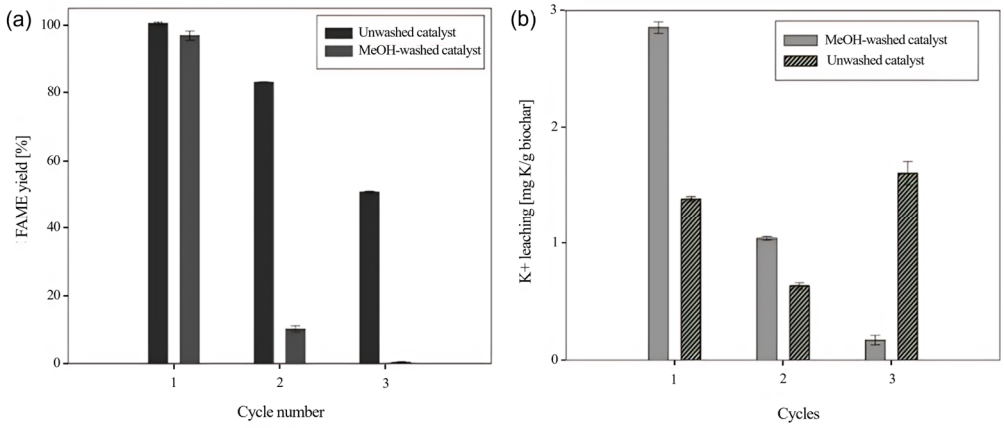

Figure 6. (**a**) FAME yield during catalyst reuse; (**b**) potassium leaching in each cycle (present in the biodiesel wash water).

For unwashed catalysts, FAME yield decreased significantly from 100% in the first cycle to approximately 51% by the third cycle, marking a 49% reduction in catalytic activity. In the case of methanol-washed catalysts, the initial FAME yield started at around 97% but decreased by about 15% after the second cycle, becoming undetectable by the third cycle.

The decline in catalytic activity in both cases was attributed to potassium leaching from the active sites into the reaction medium, as shown in Figure 6b. This outcome aligns with the mechanistic hypothesis that the basic sites generated by KOH activation are primarily responsible for catalyzing the transesterification of triglycerides. However, it also

highlights the low chemical stability of potassium on the catalyst surface, which leaches into the organic phase under reaction conditions.

Previous studies, such as those by Samart et al., demonstrated that potassium leaching could be partially mitigated by employing vacuum filtration between cycles, achieving a 60% conversion to methyl esters [56]. However, washing with a methanol–ammonia solution resulted in poorer activity, with only a 44% conversion to methyl esters. These findings emphasize the need for optimization strategies to improve the catalyst's reusability and stability.

FTIR spectra of the washed and unwashed catalyst samples (Figure 7) after three cycles present the typical absorption bands of FAME including bands in the wavelength range from 2850 to 2920 cm^{-1} attributed to the C-H bond vibration; a band at 1730–1735 cm^{-1} due to ester C=O axial deformation; and a band at 720 cm^{-1} related to the (CH_2)n group [57,58]. These bands are more intense in the spectra obtained for the unwashed catalyst, which confirms the expected effect of the methanol washing step. The higher potassium leaching observed in catalysts washed with MeOH can be attributed to the differential solubility of potassium compounds in methanol, which, due to its polar nature, enhances their extraction from the catalyst surface and active sites. Additionally, MeOH washing may induce structural modifications in the catalyst, affecting the stability of potassium-containing species and promoting their leaching compared to other treatments. Furthermore, solvent–catalyst interactions in the presence of MeOH can weaken the retention of potassium within the catalyst matrix, leading to a more pronounced release under experimental conditions [59].

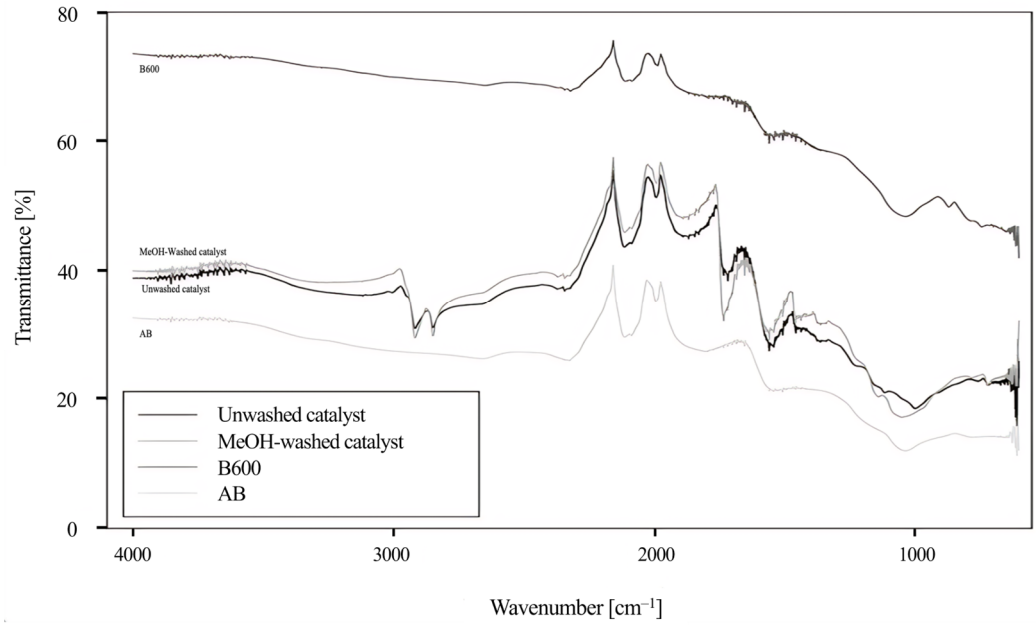

Figure 7. FITR spectra of biochar (B600), activated biochar (AB), and catalyst used after 3 cycles, unwashed and washed with methanol.

2.8. Energetic Demand and Costs Associated with the Catalyst and FAME Production

The costs and energy requirements for producing 1 kg of the catalyst are detailed in Table 7. The price of oat hulls was obtained through a quotation from a local agro-industrial company in Temuco, Chile. This consideration is significant in the context of a circular economy framework, where waste materials acquire commercial value that can fluctuate based on demand [60].

Table 7. Energy and costs required for 1 kg catalyst produced.

	Mass (kg)	Volume (L)	Price (USD)	Qs (MJ)	MJ/kg	Time (h)	Energy Required (kW)
Oat hull	4		0.23				
KOH	8		134.50				
Mixing water	10	10	0.02				
Biomass drying			0.34		7.78		
Pyrolysis			1.39		32.40	3	3
HCl 1N	8.16	8	39.30	545.62	545.62		
Wash water	24	24	0.89	7022.40	7022.4		
Catalysts drying			0.34		7.78		
Total			176.97		7615.9		

Among the inputs, KOH and HCl had the greatest impact on the final catalyst cost due to the high mass ratios required during biochar activation and neutralization processes. On the energy side, the neutralization step of activated biochar represented the highest energy demand. This was calculated based on the sensible heat needed to raise the temperature of distilled water and HCl to 90 °C.

Comparison with previous research highlights that this catalyst has a higher price per kilogram but a lower energy demand compared to the previously produced acid catalyst [43]. The increased cost is attributed to recent price hikes for KOH and HCl. However, the reduced energy demand is a result of lower water consumption, which could lead to a lower environmental impact for this catalyst. These trade-offs underline the importance of balancing cost efficiency and environmental sustainability in catalyst production.

The production of 1 kg of FAMEs (Table 8) using the present catalyst proves to be more cost-effective compared to the previously developed catalyst [43], due to the high yield (100%) achieved under optimal conditions and the short reaction time (1 min). This efficiency in the reaction process suggests that scaling up production could lead to faster and more economical biodiesel production in the future. While microwave-assisted biodiesel production has made substantial progress at the laboratory and pilot scales [61,62], its industrial application remains limited due to challenges such as optimizing reaction conditions, achieving uniform heat distribution, and developing advanced materials for efficient energy conversion. Additionally, improving process control and monitoring using advanced sensors remain essential [63–65]. This study contributes to addressing these challenges by focusing on process optimization and evaluating key factors that affect efficiency, all while incorporating sustainable catalysts like activated biochar, which aligns with the principles of a circular economy and reduces environmental impact.

Table 8. Energy required and associated costs for 1 kg FAMEs produced.

	Mass (kg)	Volume (L)	Price (USD)	Qs (MJ)	Q_L (MJ)	Et (MJ)	Energy Required (kW)
Catalyst	0.025		4.43				
WCO	1	1.1	0.44				
Methanol	0.38	0.49	4.03	126.46	0.42	126.88	
Microwave			<0.01			0.01	0.20
Total			8.90			126.90	

3. Materials and Methods

3.1. Activated Biochar Production

Chemical activation of oat hull biomass was conducted through wet impregnation using potassium hydroxide (Winkler, Heidelberg, Germany, >85%). For this process, 50 g of oat hull biomass (sieved to 300 µm with an ASTM No. 50 sieve) was mixed with KOH pellets at varying mass ratios (0.5 to 2), suspended in 500 mL of deionized water, and stirred at 300 rpm at room temperature for 24 h. Following impregnation, the suspension was filtered, and the solids were dried at 105 °C for 12 h. Subsequently, 25 g of the impregnated oat hull biomass was loaded into a pilot-scale electric pyrolyzer and subjected to carbonization under nitrogen flow (1 L/min) at a heating rate of 3.0 °C/min, following the experimental design parameters outlined in Table 9. After pyrolysis, the activated biochar samples were treated with 100 mL of 1 N HCl (Merck, Darmstadt, Germany, 37%) solution at 90 ± 3 °C for 30 min to leach out residual activating agents. The samples were then washed with distilled water multiple times until reaching a neutral pH; they were subsequently dried at 105 ± 3 °C for 24 h and were ready for further use as catalysts. A three-level factorial design (−1, 0, +1) was implemented to investigate the effects of pyrolysis conditions on biochar characteristics. The factors evaluated included pyrolysis temperature (X_1), pyrolysis time (X_2), and KOH/biomass ratio (X_3), as shown in Table 9. Statistical analyses were performed using Design Expert 6.0 software (Stat-Ease, Minneapolis, MN, USA), focusing on the surface area (Y_{BET}) as the response variable. For comparison, raw oat hull biomass without pretreatment was used as a control and pyrolyzed at 600 °C for 3 h (referred to as B600). Our research group has previously reported the characterization of this sample [43].

Table 9. Matrix of the 2^3 factorial designs adopted for the activated biochar (AB) production.

Level		Factors		
		X_1 Temperature (°C)	**X_2 Residence Time (h)**	**X_3 KOH/Biomass Ratio**
Low (−1)		400	1.0	0.5
Middle (0)		500	2.0	1.25
High (+1)		600	3.0	2.0
Run	**Identification Sample**	**X_1 (°C)**	**X_2 (h)**	**X_3**
1	AB1	600	1	2
2	AB2	400	1	0.5
3	AB3	500	2	1.25
4	AB4	400	3	0.5
5	AB5	400	3	2
6	AB6	500	2	1.25
7	AB7	600	3	0.5
8	AB8	500	2	1.25
9	AB9	400	1	2
10	AB10	600	3	2
11	AB11	600	1	0.5

3.2. Characterization of Activated Biochar

The elemental composition of the activated biochar, including carbon (C), nitrogen (N), hydrogen (H), and sulfur (S), was determined using an elemental analyzer (CHNS-O, Eurovector EA 3000, Eurovector, Pavia, Italy). The oxygen content was calculated by difference, following the method outlined in [43]. The specific surface area was measured using the BET (Brunauer–Emmett–Teller) method, while pore volume and average pore size distribution were analyzed using the BJH (Barrett–Joyner–Halenda) method. BET surface area determination is based on the formation of multiple adsorption layers, while the BJH method is based on the principle of capillary condensation and nitrogen desorption. These parameters were determined with a NOVA 1000e Quantachrome porosimeter (Aaron

Instruments, Chennai, India, nitrogen adsorption at 77 K) after preconditioning the samples by outgassing at 160 °C for 16 h. Surface functional groups were analyzed using an FTIR-ATR spectrometer (Agilent Cary 630, Agilent Technologies, Santa Clara, CA, USA), and the surface morphology was examined using a scanning electron microscope (SEM, Hitachi SU 3500, Hitachi, Tokyo, Japan). To quantify potassium content, the biochar samples were ground, calcined at 550 °C, and digested with a mixture of H_2O, HCl, and HNO_3 (8:1:1 $v/v/v$). Potassium in the digested extracts was analyzed using atomic absorption spectrometry (UNICAM Solar 969, Labexchange—Die Laborgerätebörse GmbH, Burladingen, Germany).

3.3. Biodiesel Production

Waste cooking oil (WCO) obtained from a restaurant in Temuco, Chile, was used in this study. The transesterifiable lipid content (81.70%) and other properties of the WCO were reported in a previous study [43]. Methanol and WCO were used as the reactants for biodiesel synthesis, with methanol acting as the acyl acceptor. The activated biochar catalyst, whose synthesis was explained in Section 3.1, was used as a catalyst at a dosage of 10% by mass of the oil, while the molar ratio of MeOH/WCO was set to 10:1. The catalyst used was the biochar sample with the highest specific surface area identified in Section 2.1. Kinetic experiments were conducted to determine the reaction time required to achieve maximum conversion of WCO to fatty acid methyl esters (FAMEs). These experiments were performed at 200 °C in a microwave CEM Discover Sp reactor (CEM Corporation, Matthews, NC, USA), for 1, 2, 3, 4, 5, 10, and 15 min, where the reaction power was set at 250 W. The effects of three primary factors, temperature (T), catalyst dosage (C), and WCO/MeOH molar ratio (R) on biodiesel yield, were evaluated using a factorial experimental design (Table 10). The reusability of the activated biochar-based catalyst was assessed by recovering the catalyst and repeating the reaction under the optimal conditions identified in the experimental design. Catalyst recovery was achieved by centrifugation at 6000 rpm for 10 min. The conversion efficiency was determined based on the FAME yield, which was quantified using gas chromatography (GC) equipped with a flame ionization detector (FID).

Table 10. Matrix of the 2^3 factorial design adopted in the biodiesel production using activated biochar (AB).

Level		Factors		
		X_1 Temperature (°C)	X_2 Catalyst Dosage (%)	X_3 WCO/MeOH Molar Ratio
Low (−1)		150	2.5	1/12
Middle (0)		200	6.25	1/30
High (+1)		250	10	1/48
Run	**Identification Sample**	**X_1 (°C)**	**X_2 (%)**	**X_3**
1	B1	200	6.25	1/30
2	B2	250	10	1/12
3	B3	250	2.5	1/48
4	B4	150	2.5	1/12
5	B5	250	10	1/12
6	B6	250	2.5	1/48
7	B7	150	10	1/12
8	B8	150	10	1/48
9	B9	200	6.25	1/30
10	B10	150	10	1/48
11	B11	250	2.5	1/48
12	B12	150	2.5	1/12
13	B13	150	2.5	1/12
14	B14	200	6.25	1/30
15	B15	250	10	1/48

3.4. FAME Determination

The percentage and concentration of FAMEs in the samples were determined following a method adapted from EN-14103, utilizing gas chromatography with internal calibration. A Perkin Elmer Clarus 600 gas chromatograph (GC/MS) equipped with an Elite-5MS capillary column (30 m length, 0.1 µm thickness, 0.25 mm internal diameter) was employed for the analysis (PerkinElmer, Waltham, MA, USA). Sample vials were prepared by adding 10 µL of the biodiesel sample to 233 µL of methyl heptadecanoate, which served as the internal standard at an initial concentration of 2060 mg/L. The $FAME_{yield}$ was calculated using Equation (14):

$$\%FAME_{yield}(wt\%) = \frac{FAME_{yield}(wt\%)}{TFA(wt\%)} \times 100 \quad (14)$$

where FAME represents the quantification by GC-FID, and TFA corresponds to the gravimetric quantification of transesterifiable lipids (81.70%). These compounds were determined by alkaline saponification and subsequent esterification into fatty acid methyl esters (FAMEs) according to AOCS method (Ce 2–66).

3.5. Energetic Demand and Costs Associated with the Catalyst and FAME Production

This analysis was estimated through market prices of reactive and electricity, according to the proportional mass and energy to produce 1 kg of catalyst and FAMEs under optimal reaction parameters. These estimates were made based on the structure published in our previous study [43].

4. Conclusions

To increase the production yield of FAMEs, improve the interaction of the catalyst in the reaction medium, and decrease the reaction time, activated biochar with a high specific surface area was successfully produced using oat hull biomass as a precursor and KOH as an activating agent through a chemical activation and pyrolysis process. The study showed that increasing the KOH/biomass ratio enhanced the intermediate activation reactions, resulting in a catalyst with a highly porous structure. This catalyst demonstrated high efficiency in transforming used cooking oil into biodiesel, achieving 100% conversion in just one minute using microwave assistance, with a production cost of USD 8.9 per kilogram of FAMEs. These results broaden the scope of the study, focusing on the optimization of catalyst addition and cost reduction. This research highlights the potential of utilizing residual biomass to develop reusable and sustainable catalysts, offering a promising approach for the efficient and environmentally friendly production of biodiesel.

Supplementary Materials: The following supporting information can be downloaded at: https://www.mdpi.com/article/10.3390/catal15080729/s1, Figure S1. N_2 adsorption-desorption isotherm of the samples: (A) AB1–AB4, (B) AB5–AB8, and (C) AB9–AB11. Figure S2. Pore size distribution curves of samples: (A) AB1–AB4, (B) AB5–AB8, and (C) AB9–AB11.

Author Contributions: J.Ñ.: writing, editing, investigation. B.N.: data curation, editing. K.G.-M. and N.A.: editing, analysis, visualization. M.E.G. and M.C.: supervision, resources, methodology, review. S.M.: editing, data curation. J.M.R.-G.: editing, formal analysis. All authors have read and agreed to the published version of the manuscript.

Funding: This research was funded by FONDECYT N° 11180752.

Data Availability Statement: The data presented in this study are available on request from the corresponding author. The data are not publicly available due to privacy.

Acknowledgments: ANID scholarship N° 21211437.

Conflicts of Interest: The authors declare no conflicts of interest.

References

1. Halkos, G.; Gkampoura, E.C. Assessing Fossil Fuels and Renewables' Impact on Energy Poverty Conditions in Europe. *Energies* **2023**, *16*, 560. [CrossRef]
2. Child, M.; Kemfert, C.; Bogdanov, D.; Breyer, C. Flexible Electricity Generation, Grid Exchange and Storage for the Transition to a 100% Renewable Energy System in Europe. *Renew. Energy* **2019**, *139*, 80–101. [CrossRef]
3. Vohra, K.; Vodonos, A.; Schwartz, J.; Marais, E.A.; Sulprizio, M.P.; Mickley, L.J. Global Mortality from Outdoor Fine Particle Pollution Generated by Fossil Fuel Combustion: Results from GEOS-Chem. *Environ. Res.* **2021**, *195*, 110754. [CrossRef] [PubMed]
4. UN. *Paris Agreement*; United Nations: New York, NY, USA, 2015; pp. 1–27.
5. Smith, C.J.; Forster, P.M.; Allen, M.; Fuglestvedt, J.; Millar, R.J.; Rogelj, J.; Zickfeld, K. Current Fossil Fuel Infrastructure Does Not yet Commit Us to 1.5 °C Warming. *Nat. Commun.* **2019**, *10*, 101. [CrossRef]
6. Corro, G.; Flores, A.; Pacheco-Aguirre, F.; Pal, U.; Bañuelos, F.; Ramirez, A.; Zehe, A. Biodiesel and Fossil-Fuel Diesel Soot Oxidation Activities of Ag/CeO_2 Catalyst. *Fuel* **2019**, *250*, 17–26. [CrossRef]
7. Knothe, G.; Razon, L.F. Biodiesel Fuels. *Prog. Energy Combust. Sci.* **2017**, *58*, 36–59. [CrossRef]
8. Zulqarnain; Yusoff, M.H.M.; Ayoub, M.; Hamza Nazir, M.; Zahid, I.; Ameen, M.; Abbas, W.; Shoparwe, N.F.; Abbas, N. Comprehensive Review on Biodiesel Production from Palm Oil Mill Effluent. *ChemBioEng Rev.* **2021**, *8*, 439–462. [CrossRef]
9. Muanruksa, P.; Wongsirichot, P.; Winterburn, J.; Kaewkannetra, P. Integrated Cleaner Biocatalytic Process for Biodiesel Production from Crude Palm Oil Comparing to Refined Palm Oil. *Catalysts* **2021**, *11*, 734. [CrossRef]
10. Barreiros, T.; Young, A.; Cavalcante, R.; Queiroz, E. Impact of Biodiesel Production on a Soybean Biorefinery. *Renew. Energy* **2020**, *159*, 1066–1083. [CrossRef]
11. Sahar; Sadaf, S.; Iqbal, J.; Ullah, I.; Bhatti, H.N.; Nouren, S.; Habib-ur-Rehman; Nisar, J.; Iqbal, M. Biodiesel Production from Waste Cooking Oil: An Efficient Technique to Convert Waste into Biodiesel. *Sustain. Cities Soc.* **2018**, *41*, 220–226. [CrossRef]
12. Wang, B.; Wang, B.; Shukla, S.K.; Wang, R. Enabling Catalysts for Biodiesel Production via Transesterification. *Catalysts* **2023**, *13*, 740. [CrossRef]
13. Foroutan, R.; Peighambardoust, S.J.; Mohammadi, R.; Peighambardoust, S.H.; Ramavandi, B. Application of Waste Chalk/$CoFe_2O_4$/K_2CO_3 Composite as a Reclaimable Catalyst for Biodiesel Generation from Sunflower Oil. *Chemosphere* **2022**, *289*, 133226. [CrossRef]
14. Tobío-Pérez, I.; Domínguez, Y.D.; Machín, L.R.; Pohl, S.; Lapuerta, M.; Piloto-Rodríguez, R. Biomass-Based Heterogeneous Catalysts for Biodiesel Production: A Comprehensive Review. *Int. J. Energy Res.* **2022**, *46*, 3782–3809. [CrossRef]
15. Balajii, M.; Niju, S. Biochar-Derived Heterogeneous Catalysts for Biodiesel Production. *Environ. Chem. Lett.* **2019**, *17*, 1447–1469. [CrossRef]
16. He, Y.; Chen, X.; Tang, X.; Chen, S.; Evrendilek, F.; Chen, T.; Dai, W.; Liu, J. Co-Combustion Dynamics and Products of Textile Dyeing Sludge with Waste Rubber versus Polyurethane Tires of Shared Bikes. *J. Environ. Chem. Eng.* **2023**, *11*, 109196. [CrossRef]
17. Mo, Z.; He, Y.; Liu, J.; Tu, J.; Li, D.; Hu, C.; Zhang, Q.; Wang, K.; Wang, T. Biomass Steam Gasification for Hydrogen-Rich Syngas Production over Fly Ash-Based Catalyst Pretreated by Coupling of Washing and Calcination. *Int. J. Hydrogen Energy* **2024**, *49*, 164–176. [CrossRef]
18. Joshi, N.C.; Sinha, S.; Bhatnagar, P.; Nath, Y.; Negi, B.; Kumar, V.; Gururani, P. A Concise Review on Waste Biomass Valorization through Thermochemical Conversion. *Curr. Res. Microb. Sci.* **2024**, *6*, 100237. [CrossRef]
19. Okolie, J.A.; Epelle, E.I.; Tabat, M.E.; Orivri, U.; Amenaghawon, A.N.; Okoye, P.U.; Gunes, B. Waste Biomass Valorization for the Production of Biofuels and Value-Added Products: A Comprehensive Review of Thermochemical, Biological and Integrated Processes. *Process Saf. Environ. Prot.* **2022**, *159*, 323–344. [CrossRef]
20. Chen, W.; Meng, J.; Han, X.; Lan, Y.; Zhang, W. Past, Present, and Future of Biochar. *Biochar* **2019**, *1*, 75–87. [CrossRef]
21. Hossain, M.Z.; Bahar, M.M.; Sarkar, B.; Donne, S.W.; Ok, Y.S.; Palansooriya, K.N.; Kirkham, M.B.; Chowdhury, S.; Bolan, N. Biochar and Its Importance on Nutrient Dynamics in Soil and Plant. *Biochar* **2020**, *2*, 379–420. [CrossRef]
22. Lee, J.; Kim, K.H.; Kwon, E.E. Biochar as a Catalyst. *Renew. Sustain. Energy Rev.* **2017**, *77*, 70–79. [CrossRef]
23. Srivastav, A.L.; Pham, T.D.; Izah, S.C.; Singh, N.; Singh, P.K. Biochar Adsorbents for Arsenic Removal from Water Environment: A Review. *Bull. Environ. Contam. Toxicol.* **2022**, *108*, 616–628. [CrossRef]
24. Ghanbarpour Mamaghani, Z.; Hawboldt, K.A.; MacQuarrie, S. Adsorption of CO_2 Using Biochar—Review of the Impact of Gas Mixtures and Water on Adsorption. *J. Environ. Chem. Eng.* **2023**, *11*, 109643. [CrossRef]
25. Jung, J.M.; Oh, J.I.; Baek, K.; Lee, J.; Kwon, E.E. Biodiesel Production from Waste Cooking Oil Using Biochar Derived from Chicken Manure as a Porous Media and Catalyst. *Energy Convers. Manag.* **2018**, *165*, 628–633. [CrossRef]

26. Azman, N.S.; Khairuddin, N.; Tengku Azmi, T.S.M.; Seenivasagam, S.; Hassan, M.A. Application of Biochar from Woodchip as Catalyst Support for Biodiesel Production. *Catalysts* **2023**, *13*, 489. [CrossRef]
27. Farouk, S.M.; Tayeb, A.M.; Abdel-Hamid, S.M.S.; Osman, R.M. Recent Advances in Transesterification for Sustainable Biodiesel Production, Challenges, and Prospects: A Comprehensive Review. *Environ. Sci. Pollut. Res.* **2024**, *31*, 12722–12747. [CrossRef]
28. Yadav, N.; Yadav, G.; Ahmaruzzaman, M. Fabrication of Surface-Modified Dual Waste-Derived Biochar for Biodiesel Production by Microwave-Assisted Esterification of Oleic Acid: Optimization, Kinetics, and Mechanistic Studies. *Renew. Energy* **2023**, *218*, 119308. [CrossRef]
29. Sultana, M.; Ahmaruzzaman, M. Transforming Waste Biomass to a Heterogenous Acid Catalyst for Microwave-Assisted Biodiesel Production: Empirical Evaluation and Kinetic Study. *Biomass Convers. Biorefin.* **2025**, *10*, 1–19. [CrossRef]
30. Bizualem, Y.D.; Nurie, A.G. A Review on Recent Biodiesel Intensification Process through Cavitation and Microwave Reactors: Yield, Energy, and Economic Analysis. *Heliyon* **2024**, *10*, e24643. [CrossRef]
31. Wang, J.; Kaskel, S. KOH Activation of Carbon-Based Materials for Energy Storage. *J. Mater. Chem.* **2012**, *22*, 23710–23725. [CrossRef]
32. Monteagudo, J.M.; Durán, A.; Alonso, M.; Stoica, A.I. Investigation of Effectiveness of KOH-Activated Olive Pomace Biochar for Efficient Direct Air Capture of CO_2. *Sep. Purif. Technol.* **2025**, *352*, 127997. [CrossRef]
33. Liu, Y.; Liu, P.; Li, L.; Wang, S.; Pan, Z.; Song, C.; Wang, T. Fabrication of Biomass-Derived Activated Carbon with Interconnected Hierarchical Architecture via H_3PO_4-Assisted KOH Activation for High-Performance Symmetrical Supercapacitors. *J. Electroanal. Chem.* **2021**, *903*, 115828. [CrossRef]
34. Mitome, T.; Uchida, Y.; Egashira, Y.; Hayashi, K.; Nishiura, A.; Nishiyama, N. Adsorption of Indole on KOH-Activated Mesoporous Carbon. *Colloids Surf. A Physicochem. Eng. Asp.* **2013**, *424*, 89–95. [CrossRef]
35. Khamkeaw, A.; Asavamongkolkul, T.; Perngyai, T.; Jongsomjit, B.; Phisalaphong, M. Interconnected Micro, Meso, and Macro Porous Activated Carbon from Bacterial Nanocellulose for Superior Adsorption Properties and Effective Catalytic Performance. *Molecules* **2020**, *25*, 4063. [CrossRef]
36. Sevilla, M.; Díez, N.; Fuertes, A.B. More Sustainable Chemical Activation Strategies for the Production of Porous Carbons. *ChemSusChem* **2021**, *14*, 94–117. [CrossRef]
37. Chen, W.; Gong, M.; Li, K.; Xia, M.; Chen, Z.; Xiao, H.; Fang, Y.; Chen, Y.; Yang, H.; Chen, H. Insight into KOH Activation Mechanism during Biomass Pyrolysis: Chemical Reactions between O-Containing Groups and KOH. *Appl. Energy* **2020**, *278*, 115730. [CrossRef]
38. Zhang, Y.; Zhao, Y.P.; Qiu, L.L.; Xiao, J.; Wu, F.P.; Cao, J.P.; Bai, Y.H.; Liu, F.J. Insights into the KOH Activation Parameters in the Preparation of Corncob-Based Microporous Carbon for High-Performance Supercapacitors. *Diam. Relat. Mater.* **2022**, *129*, 109331. [CrossRef]
39. Gale, M.; Nguyen, T.; Moreno, M.; Gilliard-Abdulaziz, K.L. Physiochemical Properties of Biochar and Activated Carbon from Biomass Residue: Influence of Process Conditions to Adsorbent Properties. *ACS Omega* **2021**, *6*, 10224–10233. [CrossRef]
40. Schmitz, E.; Karlsson, E.N.; Adlercreutz, P.; Schmitz, C.E.; Leegood, E.R. Warming Weather Changes the Chemical Composition of Oat Hulls. *Plant Biol.* **2020**, *22*, 1086–1091. [CrossRef]
41. Martinez-Toledo, C.; Valdes-Vidal, G.; Calabi-Floody, A.; Gonzalez, M.E.; Reyes-Ortiz, O. Evaluation of Rheological Properties of Asphalt Binder Modified with Biochar from Oat Hulls. *Materials* **2024**, *17*, 4312. [CrossRef]
42. Han, L.P.; Wang, W.H.; Eneji, A.E.; Liu, J. Phytoremediating Coastal Saline Soils with Oats: Accumulation and Distribution of Sodium, Potassium, and Chloride Ions in Plant Organs. *J. Clean. Prod.* **2015**, *90*, 73–81. [CrossRef]
43. González, M.E.; Cea, M.; Reyes, D.; Romero-Hermoso, L.; Hidalgo, P.; Meier, S.; Benito, N.; Navia, R. Functionalization of Biochar Derived from Lignocellulosic Biomass Using Microwave Technology for Catalytic Application in Biodiesel Production. *Energy Convers. Manag.* **2017**, *137*, 165–173. [CrossRef]
44. Vasić, K.; Podrepšek, G.H.; Knez, Ž.; Leitgeb, M. Biodiesel Production Using Solid Acid Catalysts Based on Metal Oxides. *Catalysts* **2020**, *10*, 237. [CrossRef]
45. Olutoye, M.A.; Hameed, B.H. Kinetics and Deactivation of a Dual-Site Heterogeneous Oxide Catalyst during the Transesterification of Crude Jatropha Oil with Methanol. *J. Taibah Univ. Sci.* **2016**, *10*, 685–699. [CrossRef]
46. Chaos-Hernández, D.; Reynel-Avila, H.E.; Mendoza-Castillo, D.I.; Bonilla-Petriciolet, A.; Aguayo-Villarreal, I.A. Functionalization and Activation of Carbon-Based Catalysts with KOH and Calcium and Their Application in Transesterification to Produce Biodiesel: Optimization of Catalytic Properties and Kinetic Study. *Fuel* **2022**, *310*, 122066. [CrossRef]
47. Sarve, A.N.; Varma, M.N.; Sonawane, S.S. Ultrasound Assisted Two-Stage Biodiesel Synthesis from Non-Edible Schleichera Triguga Oil Using Heterogeneous Catalyst: Kinetics and Thermodynamic Analysis. *Ultrason. Sonochem* **2016**, *29*, 288–298. [CrossRef]
48. Wang, S.; Yuan, H.; Wang, Y.; Shan, R. Transesterification of Vegetable Oil on Low Cost and Efficient Meat and Bone Meal Biochar Catalysts. *Energy Convers. Manag.* **2017**, *150*, 214–221. [CrossRef]

49. Osman, A.I.; Ayati, A.; Krivoshapkin, P.; Tanhaei, B.; Farghali, M.; Yap, P.S.; Abdelhaleem, A. Coordination-Driven Innovations in Low-Energy Catalytic Processes: Advancing Sustainability in Chemical Production. *Coord. Chem. Rev.* **2024**, *514*, 215900. [CrossRef]
50. Motasemi, F.; Ani, F.N. A Review on Microwave-Assisted Production of Biodiesel. *Renew. Sustain. Energy Rev.* **2012**, *16*, 4719–4733. [CrossRef]
51. Patil, P.D.; Gude, V.G.; Reddy, H.K.; Muppaneni, T.; Deng, S.; Patil, P.D.; Gude, V.G.; Reddy, H.K.; Muppaneni, T.; Deng, S. Biodiesel Production from Waste Cooking Oil Using Sulfuric Acid and Microwave Irradiation Processes. *J. Environ. Prot.* **2012**, *3*, 107–113. [CrossRef]
52. Hincapié, G.M.; Valange, S.; Barrault, J.; Moreno, J.A.; López, D.P. Effect of Microwave-Assisted System on Transesterification of Castor Oil with Ethanol. *Univ. Sci.* **2014**, *19*, 193–200. [CrossRef]
53. Salema, A.A.; Yeow, Y.K.; Ishaque, K.; Ani, F.N.; Afzal, M.T.; Hassan, A. Dielectric Properties and Microwave Heating of Oil Palm Biomass and Biochar. *Ind. Crops Prod.* **2013**, *50*, 366–374. [CrossRef]
54. Devasan, R.; Ruatpuia, J.V.L.; Gouda, S.P.; Kodgire, P.; Basumatary, S.; Halder, G.; Rokhum, S.L. Microwave-Assisted Biodiesel Production Using Bio-Waste Catalyst and Process Optimization Using Response Surface Methodology and Kinetic Study. *Sci. Rep.* **2023**, *13*, 2570. [CrossRef]
55. Kataria, J.; Mohapatra, S.K.; Kundu, K. Biodiesel Production from Frying Oil Using Zinc-Doped Calcium Oxide as Heterogeneous Catalysts. *Energy Sources Part A Recovery Util. Environ. Eff.* **2017**, *39*, 861–866. [CrossRef]
56. Samart, C.; Sreetongkittikul, P.; Sookman, C. Heterogeneous Catalysis of Transesterification of Soybean Oil Using KI/Mesoporous Silica. *Fuel Process. Technol.* **2009**, *90*, 922–925. [CrossRef]
57. Janu, R.; Mrlik, V.; Ribitsch, D.; Hofman, J.; Sedláček, P.; Bielská, L.; Soja, G. Biochar Surface Functional Groups as Affected by Biomass Feedstock, Biochar Composition and Pyrolysis Temperature. *Carbon Resour. Convers.* **2021**, *4*, 36–46. [CrossRef]
58. Huang, H.; Tang, J.; Gao, K.; He, R.; Zhao, H.; Werner, D. Characterization of KOH Modified Biochars from Different Pyrolysis Temperatures and Enhanced Adsorption of Antibiotics. *RSC Adv.* **2017**, *7*, 14640–14648. [CrossRef]
59. Stoytcheva, M.; Montero, G.; Stoytcheva, M.; Montero, G. *Biodiesel—Feedstocks and Processing Technologies*; IntechOpen Limited: London, UK, 2011. [CrossRef]
60. Antonioli, D.; Ghisetti, C.; Mazzanti, M.; Nicolli, F. Sustainable Production: The Economic Returns of Circular Economy Practices. *Bus. Strategy Environ.* **2022**, *31*, 2603–2617. [CrossRef]
61. Demir, V.G.; Yuksel, H.; Koten, H.; Zafer Gul, M.; Soyhan, H.S. Microwave-Assisted Pilot-Scale Biodiesel Production and Engine Tests. *Proc. Inst. Civ. Eng.-Energy* **2019**, *172*, 1–11. [CrossRef]
62. Rhithuparna, D.; Ghosh, N.; Lalthazuala Rokhum, S.; Halder, G. Current Progress and Future Outlooks of Microwave-Irradiated Biodiesel Production: A Holistic Review. *Chem. Eng. J.* **2024**, *482*, 149033. [CrossRef]
63. Dąbrowska, S.; Chudoba, T.; Wojnarowicz, J.; Łojkowski, W. Current Trends in the Development of Microwave Reactors for the Synthesis of Nanomaterials in Laboratories and Industries: A Review. *Crystals* **2018**, *8*, 379. [CrossRef]
64. Tapia-Quirós, P.; Granados, M.; Sentellas, S.; Saurina, J. Microwave-Assisted Extraction with Natural Deep Eutectic Solvents for Polyphenol Recovery from Agrifood Waste: Mature for Scaling-Up? *Sci. Total Environ.* **2024**, *912*, 168716. [CrossRef] [PubMed]
65. Liow, M.Y.; Gourich, W.; Chang, M.Y.; Loh, J.M.; Chan, E.S.; Song, C.P. Towards Rapid and Sustainable Synthesis of Biodiesel: A Review of Effective Parameters and Scale-up Potential of Intensification Technologies for Enzymatic Biodiesel Production. *J. Ind. Eng. Chem.* **2022**, *114*, 1–18. [CrossRef]